Research in Astronomy and Astrophysics, 25:075002 (10pp), 2025 July

https://doi.org/10.1088/1674-4527/adda7e
CSTR: 32081.14.RAA.adda7e

Joint Constraint on the Jet Structure from the Short GRB Population and GRB 170817A

Xiao-Feng Cao[1], Wei-Wei Tan[1], Yun-Wei Yu[2,3,4], and Zhen-Dong Zhang[5]
[1] Institute of Astronomy and High Energy Physics, Hubei University of Education, Wuhan 430205, China; caoxiaofeng@hue.edu.cn, wwtan@hue.edu.cn
[2] Institute of Astrophysics, Central China Normal University, Wuhan 430079, China; yuyw@ccnu.edu.cn
[3] Key Laboratory of Quark and Lepton Physics (Central China Normal University), Ministry of Education, Wuhan 430079, China
[4] Education Research and Application Center, National Astronomical Data Center, Wuhan 430079, China
[5] Department of Physics and Astronomy, University of Tennessee, Knoxville, TN 37996-1200, USA
Received 2025 March 5; revised 2025 May 6; accepted 2025 May 16; published 2025 June 12

Abstract

The nearest GRB 170817A provided an opportunity to probe the angular structure of the jet of this short gamma-ray burst (SGRB), by using its off-axis observed afterglow emission. It is investigated whether the afterglow-constrained jet structures can be consistent with the luminosity of the prompt emission of GRB 170817A. Furthermore, by assuming that all SGRBs, including GRB 170817A, have the same explosive mechanism and jet structure, we apply the different jet structures to the calculation of the flux and redshift distributions of the SGRB population, confronting them with the observational distributions of the Swift and Fermi sources. In comparison, it is found that the power-law and double-Gaussian models could be somewhat more favored than the single-Gaussian structure, as the last one could not be very consistent with the flux distribution of the Fermi data. Nevertheless, in view of the large uncertainty of parameters, we are still unable to make a sufficiently conclusive judgement at present.

Key words: (stars:) gamma-ray burst: general – (stars:) gamma-ray burst: individual (GRB 170817A) – stars: jets

1. Introduction

Gamma-ray bursts (GRBs) are generated by highly beamed relativistic jets, which are driven by rapidly rotating black hole or neutron star engines. Before gamma-ray emission is produced, the jets should first propagate through dense progenitor material, which can be a stellar envelope for long GRBs (Matzner 2003; Zhang et al. 2003; Lazzati & Begelman 2005; Bromberg et al. 2011, 2014; Suwa & Ioka 2011; Yu 2020; Gottlieb & Nakar 2022; Urrutia et al. 2023a, 2023b) or a merger ejecta for short GRBs (SGRBs; Nagakura et al. 2014; Lazzati et al. 2017; Yu 2020; Hamidani & Ioka 2021; Nathanail et al. 2021; Gottlieb & Nakar 2022; Nativi et al. 2022; Pavan et al. 2023).

As a result of its interaction with the progenitor material, a GRB jet breaking out from the progenitor can finally own an angular structure for its energy and velocity distributions. Generally speaking, the breakout jet can consist of a core region with an opening angle of a few degrees and a relatively wider and less energetic wing region (Lazzati et al. 2018; Salafia & Ghirlanda 2022). In addition, the jet can also be surrounded by a much wider cocoon that is contributed by the shocked material. Nevertheless, it seems unnecessary to treat the jet and cocoon separately, due to the mixing of the material and the continuous distribution of the energy. Instead, we can simply treat the cocoon as a part of the jet wing. From the core to the wing, the Lorentz factor and the energy density of the jet can decrease rapidly with the increasing angle relative to the jet axis. Three empirical analytical functions have usually been suggested to describe the angular structure of GRB jets, including a power-law (Dai & Gou 2001; Zhang & Mészáros 2002; Kumar & Granot 2003; Lazzati & Begelman 2005), a Gaussian (Rossi et al. 2002, 2004; Zhang & Mészáros 2002; Granot & Kumar 2003; Kumar & Granot 2003), and, sometimes, double Gaussians (Tan & Yu 2020; Luo et al. 2022; Wei et al. 2022).

Observational constraints on the jet structures can, in principle, provide a clue to understand the nature and interior of GRB progenitors. First, a direct implication for the angular structure can be derived from the afterglow emission of GRBs, particularly when the viewing direction significantly deviates from the jet axis (Kumar & Granot 2003). Because of the relativistic beaming effect, the emission from the jet material deviating from the line of sight (LOS) can be detected only after the material is decelerated to have an emission beaming angle larger than the viewing angle. Therefore, it can be expected that the more luminous emission from more energetic jet material can be detected later for an off-axis observation. In this case, the peak of the afterglow light curves can appear when the core emission comes into sight, and the increasing light curves before the peak simply reflect the angular distribution of the jet energy density.

The problem is that, for the majority of observed GRBs, their cosmological distances always prevent us from detecting them at a large viewing angle, because of the rapid decrease of the jet energy with the angle. Without a GRB trigger, it will be very difficult to capture the orphan afterglow emission of the GRBs. Following such a consideration, the observed GRBs are always assumed to be on-axis, and a "top-hat" structure is generally appropriate for the afterglow modeling, at most, by further invoking an opening angle for the jet if a so-called jet-break feature appears in the light curves. Nevertheless, this situation has changed since the detection of the nearest GRB 170817A at a distance of $\sim$40 Mpc. The viewing angle of this GRB was quickly constrained to be about $\theta_{\rm obs} \leqslant 31^\circ$ by the gravitational wave detection of GW170817 (Abbott et al. 2017a). This special multi-messenger event provided the first opportunity to constrain the angular structure of the GRB jet by its afterglow emission and various jet structure models had been widely investigated (Lamb & Kobayashi 2017; Margutti et al. 2017, 2018; Troja et al. 2017, 2018; Xiao et al. 2017; D'Avanzo et al. 2018; Granot et al. 2018; He et al. 2018; Lazzati et al. 2018; Mooley et al. 2018; Nynka et al. 2018; Resmi et al. 2018; Xie et al. 2018; Beniamini & Nakar 2019; Huang et al. 2019; Kathirgamaraju et al. 2019; Lamb et al. 2019; Ziaeepour 2019; Beniamini et al. 2020; Takahashi & Ioka 2020, 2021; Wei et al. 2022). Besides explaining the afterglow emission, the off-axis observation of GRB 170817A also provides a natural but qualitative explanation for its ultra-low-luminosity of $\sim 10^{47}\,{\rm erg\,s^{-1}}$ (Abbott et al. 2017b; Zhang et al. 2018). Then, it needs to be checked whether the observed prompt luminosity can be quantitatively consistent with the jet structure derived from the afterglow modeling.

Furthermore, a large viewing angle of GRB 170817A is necessary to understand the very high event rate of nearby GRBs inferred from GRB 170817A. Meanwhile, a question arises here: How can we connect this nearby SGRB rate in a natural way with the rates of the other SGRBs? In more detail, if all SGRBs, including GRB 170817A, share a common geometry for their jets, then it is crucial to ask how this common jet structure influences our understanding of the observational redshift and energy distributions of all SGRBs as well as the determination of the luminosity function (LF) and event rate of the SGRBs, as previously investigated (Salafia et al. 2020; Tan & Yu 2020; Luo et al. 2022; Salafia & Ghirlanda 2022; Hayes et al. 2023). It should be noted that the luminosity can actually vary with the angle, even in the jet core region, but is not uniformly distributed as assumed in the top-hat model. Meanwhile, the LOS of SGRBs is randomly distributed and usually not strictly parallel to the jet axis. Therefore, even though some SGRBs have an identical jet, their observed luminosity can still be different and distributed within a range. In this case, if a top-hat uniform jet structure is preconceived in our mind, then we would ascribe this luminosity distribution to be a component of the LF of SGRBs. This is the reason why an apparent broken power-law LF can always be obtained. In contrast, if a realistic jet structure can be taken into account correctly, then we can find that the low-luminosity component of the apparent LF can naturally result from the random distribution of the viewing angles (Tan & Yu 2020). Meanwhile, it is completely sufficient to invoke the high-luminosity power-law to describe the distribution of the central luminosity of SGRB jets. In other words, the intrinsic LF of SGRBs can be a single power-law.

However, in the previous work, the constraints on the jet structure from the GRB 170817A observations and population statistics were usually treated separately, but have not been quantitatively confronted with each other. Therefore, this paper is devoted to investigating the consistency between these two types of observational constraints. In the next section, we briefly introduce the afterglow model and display the constrained model parameters for three typical structure functions. In Section 3, on the one hand, we derive the angular dependence of the equivalent isotropic emission energy ($E_{\gamma,\rm iso}$) from the energy density (ε) distribution of the jets, compared to the prompt luminosity of GRB 170817A. On the other hand, we compare the model-predicted redshift and flux distributions of SGRBs with the observational ones. A summary is given in Section 4.

2. Constraining Jet Structure by the Afterglows of GRB 170817A

As usual, for calculating the afterglow emission from a structured jet, we can separate the jet into a series of differential rings and the dynamical evolution of each ring can be expressed as (Huang et al. 1999; Li et al. 2019):

$$\frac{d\Gamma_\theta}{dM_{{\rm sw},\theta}} = -\frac{\Gamma_\theta^2 - 1}{M_{{\rm ej},\theta} + 2\Gamma_\theta M_{{\rm sw},\theta}}, \tag{1}$$

where Γ_θ is the Lorentz factor of the ring of an half-opening angle θ, $M_{{\rm ej},\theta}$ and $M_{{\rm sw},\theta}$ are the masses per solid angle of the GRB ejecta and the swept-up interstellar medium (ISM), respectively. Here, the possible lateral motion of the jet material is ignored, and thus the dynamical evolution of each ring can be considered independently, which has also been widely considered in previous afterglow modelings of GRB 170817A (e.g., Gill & Granot 2018; Lazzati et al. 2018; Morsony et al. 2024). It is sometimes suggested that a top-hat jet could expand laterally on the sound speed of the shocked material (e.g., Huang et al. 1999). However, numerical simulations show that this could not be true and, instead, most of the jet energy can actually remain within the initial opening angle of the jet for a long period (Zhang & MacFadyen 2009; Meliani & Keppens 2010; van Eerten et al. 2010; Granot & Piran 2012). By denoting the angular distribution of the jet kinetic energy by $\varepsilon_\theta \equiv dE_{\rm k}/d\Omega$, we have

$M_{\rm ej,\theta} = \varepsilon_\theta/\Gamma_{\theta,\rm i}c^2$, where the subscript "$i$" of $\Gamma_{\theta,\rm i}$ represents its initial value. Meanwhile, the increase of the swept-up mass is determined by

$$\frac{dM_{\rm sw,\theta}}{dr_\theta} = r_\theta^2 n m_{\rm p}, \tag{2}$$

where r_θ is the radius of the jet external shock, n is the number density of the ISM, which is considered to be constant in our calculation, and $m_{\rm p}$ is the mass of the proton.

Following Sari et al. (1998), the synchrotron luminosity contributed by a differential element of a mass $M_{\rm sw,\theta}$ can be calculated analytically as (Yu et al. 2022)

$$I'_{\nu'}(r, \theta, \varphi) = \frac{M_{\rm sw,\theta}}{r_\theta^2 m_{\rm p}} \frac{m_{\rm e}c^2\sigma_{\rm T}B'}{12\pi e} S(\nu'), \tag{3}$$

where the superscript prime indicates that the quantities are measured in the comoving frame of the shocked region, $m_{\rm e}$ is the mass of electron, c the speed of light, $\sigma_{\rm T}$ the Thomson cross section, e the electron charge, and B' represents the comoving magnetic field strength. The dimensionless synchrotron spectrum $S(\nu')$ can be expressed as a broken power-law function, which is characterized by two broken frequencies that are determined by the acceleration and cooling of electrons (see Sari et al. 1998 for details). As usual, three microphysical parameters are involved here, including the spectral index of the shock-accelerated electrons p, the equipartition factors $\epsilon_{\rm B}$ and $\epsilon_{\rm e}$ for the magnetic fields and electrons in the shocked material, respectively. Moreover, a relationship $\epsilon_{\rm e} = \sqrt{\epsilon_{\rm B}}$ will be taken in our calculation in order to reduce the degree of freedom of the model, according to the theoretical prediction given by Medvedev (2006). Then, for an observer of a viewing angle $\theta_{\rm obs}$ relative to the jet axis, the observed flux of the afterglow emission can be obtained by integrating over the whole solid angle of the jet as (Huang et al. 2000; Yu et al. 2007, 2022)

$$F_\nu(t) = \frac{r_\theta^2}{d_{\rm L}^2} \int \frac{I'_{\nu'}(r, \theta, \phi)}{\Gamma_\theta^3(1 - \beta_\theta \cos\alpha)^3} \cos\alpha d\Omega(\theta, \phi), \tag{4}$$

where $d_{\rm L}$ is the luminosity distance of the GRB, $\beta_\theta = (1 - \Gamma_\theta^{-2})^{1/2}$, and α is defined as the angle between the emitting differential element and the LOS, which can be expressed as (e.g., Li et al. 2019)

$$\cos\alpha = \cos\theta \cos\theta_{\rm obs} + \sin\theta \sin\theta_{\rm obs} \cos\phi. \tag{5}$$

Finally, the connection between the radius of emitting material and the observational time is given by $dr_\theta/dt = \beta_\theta c/(1 - \beta_\theta \cos\alpha)$.

In this paper, the following three representative functions are taken to describe the possible jet structures:

1. Power-law jet

$$\varepsilon_\theta = \varepsilon_{\rm c}\Theta^{-k_1}, \tag{6}$$

$$\Gamma_{\theta,\rm i} = \Gamma_{\rm c}\Theta^{-k_2} + 1, \tag{7}$$

with $\Theta = [1 + (\theta/\theta_{\rm c})^2]^{1/2}$;

2. Single-Gaussian jet

$$\varepsilon_\theta = \varepsilon_{\rm c} \exp\left(-\frac{\theta^2}{2\theta_{\rm c}^2}\right), \tag{8}$$

$$\Gamma_{\theta,\rm i} = \Gamma_{\rm c} \exp\left(-\frac{\theta^2}{2\theta_{\rm c}^2}\right) + 1; \tag{9}$$

3. Double-Gaussian jet

$$\varepsilon_\theta = \varepsilon_{\rm c}\left[\exp\left(-\frac{\theta^2}{2\theta_{\rm c}^2}\right) + \mathcal{C}_{\rm E} \exp\left(-\frac{\theta^2}{2\theta_{\rm out}^2}\right)\right], \tag{10}$$

$$\Gamma_{\theta,\rm i} = \Gamma_{\rm c}\left[\exp\left(-\frac{\theta^2}{2\theta_{\rm c}^2}\right) + \mathcal{C}_\Gamma \exp\left(-\frac{\theta^2}{2\theta_{\rm out}^2}\right)\right] + 1, \tag{11}$$

where the free parameters k_1, k_2, $\varepsilon_{\rm c}$, $\Gamma_{\rm c}$, $\theta_{\rm c}$, $C_{\rm E}$, C_Γ, and $\theta_{\rm out}$ can be constrained by fitting the observed afterglows of GRB 170817A. Substituting these structure functions into the dynamical equation, we calculate the afterglow light curves for arbitrary viewing angles and constrain the model parameters by confronting the observational data of GRB 170817A, as presented in Figure 1 for a direct impression.[6] Here, since the flux evolution for an off-axis observation basically traces the angular dependence of the jet properties, it is in principle possible to obtain a constraint on the structure parameters, even in the double-Gaussian case where the outer and inner Gaussian components can correspond to the early and late light curves roughly separately.

To be specific, the constraints on the model parameters are obtained with the Bayesian method, where the *emcee* package (Foreman-Mackey et al. 2013) is used within a wide range of parameter values. The priors and posteriors with 1σ errors of the parameter values are listed in Table 1, which are in good

[6] The result corresponding to the double-Gaussian case has been previously presented in Wei et al. (2022).

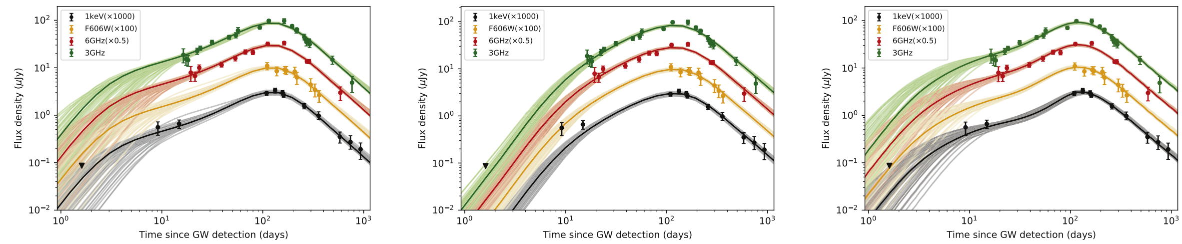

Figure 1. The fits of the multi-wavelength afterglow light curves of GRB 170817A for a power-law (left), single-Gaussian (middle), or double-Gaussian (right) jet structure. The observational data are taken from Makhathini et al. (2021).

agreement with the previous results (e.g., Gill & Granot 2018; Lazzati et al. 2018; Morsony et al. 2024). Here, the log-likelihood function is defined as $\ln\mathcal{L} = -\frac{1}{2}\sum_{i=1}^{n}\frac{(O_i - M_i)^2}{\sigma_i^2}$, where O_i are the observations, M_i are the corresponding model predictions, and σ_i are the observational uncertainties. To ensure comprehensive mixing and robust convergence of the MCMC sampling, the chains were allowed to run for more than 50 times the autocorrelation time, where the autocorrelation times were found to be approximately 100 for each parameter. Furthermore, samplings were repeated multiple times to ensure consistent convergence, leading to a reliable and reproducible solution. In view of the large number of model parameters (that is 9, 7, and 10 for the power-law, single-Gaussian, and double-Gaussian cases, respectively), the parameter constraints are always subject to a degeneracy problem (e.g., Granot & Sari 2002; Nakar & Piran 2021), which cannot be eliminated even though the *emcee* package is used (Garcia-Cifuentes et al. 2024). Then, undoubtedly, it is necessary to find more independent constraints. For example, Fong et al. (2019) measured $p = 2.166 \pm 0.026$ directly from the evolving afterglow spectra from radio to X-ray, which is not very different from our result of $p \sim (2.12–2.13)$. Moreover, the dynamical evolution of the structured jet could also be inferred from the superluminal apparent motion of the centroid of radio emission sampled by the very long-baseline interferometry (VLBI) (Mooley et al. 2018). Therefore, in the next section, we will further endeavor to constrain these jet structures according to the statistical distributions of SGRBs.

3. Confronting the Jet Structures with the Population Statistics of SGRBs

3.1. The Direction-dependence of the Emission Energy

Because of the jet structure, the emission energy inferred from the observations should highly depend on the viewing angle. Furthermore, due to the relativistic beaming of the jet emission, the observed luminosity could not always be determined by the kinetic energy of the jet in the same direction (Salafia et al. 2015). For a viewing angle $\theta_{\rm obs}$, the isotropically equivalent energy of the GRB prompt emission can be calculated by (Rybicki & Lightman 1979; Salafia et al. 2015)

$$E_{\gamma,\rm iso}(\theta_{\rm obs}) = \eta_\gamma \int \frac{\varepsilon_\theta}{\Gamma_\theta^4[1 - \beta_\theta \cos\alpha]^3} d\Omega(\theta, \phi), \tag{12}$$

where η_γ is the radiation efficiency, which is assumed to be a constant for different times and different directions. With the parameter values listed in Table 1, we plot the dependence of the emission energy on $\theta_{\rm obs}$ in Figure 2 (solid circles). Radiation efficiency η_γ can be determined by tuning the theoretical lines to be consistent with the observational data of GRB 170817A. For the central value of the parameters, we have $\eta_\gamma = 0.08$, 0.013, and 0.2 for the power-law, single-Gaussian, and double-Gaussian jet structures, respectively. The errors of the structure parameters would lead to the value of η_γ varying within a wide range, which is about an order of magnitude, as indicated by the shaded bands in Figure 2.

Generally speaking, the emission energy can roughly trace the kinetic energy for viewing angles not much larger than the jet opening angle. However, when the observational direction is far away from the jet axis, the emission energy could become much higher than the kinetic energy in the same direction, particularly in the case of a Gaussian structure. The large-angle emission is actually contributed from the jet material at smaller angles, and the prompt emission of GRB 170817A is only in such a situation. [7]

Furthermore, we derive the observational isotropic luminosity from the emission energy by using $L_{\rm iso} = E_{\gamma,\rm iso}/T$, where T is the duration of the emission. Here, for simplicity, we assume a constant value of $T \sim 1$ s for all SGRBs. Therefore, the direction-dependence of the isotropic luminosity can be described analytically by the following functions, which are obtained by fitting the $E_{\gamma,\rm iso} - \theta_{\rm obs}$ relations displayed in

[7] Since the single-Gaussian cannot directly explain the prompt emission of GRB 170817A, Tan & Yu (2020) suggested an outer Gaussian component. However, as shown here, the GRB 170817A emission actually could be explained by the large-angle emission effect, which indicates that the outer Gaussian may not be indispensable. However, in this paper, we keep considering the double-Gaussian situation, because the double-Gaussian structure could still be a natural result of the jet propagation, and it is also helpful for improving the afterglow modeling (Wei et al. 2022).

Table 1
Model Parameters Constrained from the Afterglow Modeling of GRB 170817A

Parameter	Prior	Posterior		
		Power-law	Single-Gaussian	Double-Gaussian
$\theta_{\rm obs}$/deg	(17, 35)	$22.89^{+3.71}_{-3.03}$	$23.21^{+3.95}_{-3.60}$	$19.37^{+2.21}_{-1.53}$
$\log(\varepsilon_{\rm c}/{\rm erg\ sr}^{-1})$	(48, 53)	$50.92^{+0.35}_{-0.54}$	$51.76^{+0.85}_{-0.98}$	$51.04^{+0.24}_{-0.31}$
$\log(C_{\rm E})$	(−5, 0)	/	/	$-1.33^{+0.19}_{-0.18}$
$\Gamma_{\rm c}$	(100, 600)	352^{+265}_{-174}	507^{+66}_{-103}	456^{+236}_{-235}
C_Γ	(0, 1)	/	/	$0.49^{+0.33}_{-0.30}$
$\theta_{\rm c}$/deg	(1, 10)	$2.56^{+1.08}_{-0.62}$	$3.64^{+0.63}_{-0.53}$	$1.48^{+0.41}_{-0.32}$
$\theta_{\rm out}$/deg	(2, 15)	/	/	$4.16^{+0.87}_{-0.54}$
k_1	(3, 8)	$3.97^{+0.64}_{-0.52}$	/	/
k_2	(0.1, 3)	$2.64^{+0.25}_{-0.42}$	/	/
$\log(n/{\rm cm}^{-3})$	(−4, 0)	$-2.98^{+0.49}_{-0.57}$	$-2.06^{+0.94}_{-1.01}$	$-3.19^{+0.40}_{-0.43}$
$\log(\epsilon_{\rm B})$	(−6, −1)	$-2.36^{+0.63}_{-0.46}$	$-3.98^{+1.31}_{-1.11}$	$-2.59^{+0.41}_{-0.28}$
p	(2, 2.3)	$2.13^{+0.01}_{-0.01}$	$2.12^{+0.01}_{-0.01}$	$2.13^{+0.01}_{-0.01}$

Figure 2. Specifically, for a constant duration, we have

$$L_{\rm iso}(\theta_{\rm obs}) = L_{\rm on}\frac{1+\left(\frac{\theta_{\rm obs}}{\theta_{b2}}\right)^{\alpha_3}}{\left[\left(\frac{\theta_{\rm obs}}{\theta_{b1}}\right)^{-\alpha_1 s}+\left(\frac{\theta_{\rm obs}}{\theta_{b1}}\right)^{\alpha_2 s}\right]^{1/s}} \tag{13}$$

for the power-law and single-Gaussian jets and

$$L_{\rm iso}(\theta_{\rm obs}) = L_{\rm on}\left\{\frac{1+\left(\frac{\theta_{\rm obs}}{\theta_{b2}}\right)^{\alpha_3}}{\left[\left(\frac{\theta_{\rm obs}}{\theta_{b1}}\right)^{-\alpha_1 s}+\left(\frac{\theta_{\rm obs}}{\theta_{b1}}\right)^{\alpha_2 s}\right]^{1/s}} + \mathcal{R}\exp\left(-\frac{\theta_{\rm obs}^2}{2\theta_{\rm b3}^2}\right)\right\} \tag{14}$$

for the double-Gaussian jets, where $L_{\rm on}$ is the luminosity value for the on-axis (i.e., $\theta_{\rm obs} = 0°$) observation, and other parameter values are listed in Table 2. The invoking of these two empirical functions can help us accelerate the following calculations. It should be kept in mind that the duration of SGRBs is intrinsically determined by the period of the engine activity and, furthermore, influenced by the propagation of the jet through the progenitor material. Nevertheless, ignoring these details, the ultimate distribution of the duration could be well described by a Gaussian as observed, which could not be significantly influenced by the selection effects. Compared with our constant duration assumption, the realistic distribution of the duration would lead to an extra diffusion of the values of the model parameter constrained later in this paper.

As found in Salafia et al. (2015) and Tan & Yu (2020), the $\theta_{\rm obs}$-dependence of the GRB luminosity can substantially influence the determination of the LF of SGRBs, which was usually found to have an apparent broken-power-law form (Wanderman & Piran 2015; Ghirlanda et al. 2016; Tan & Yu 2020), where the flat low-luminosity component within the luminosity range ($L_{\rm iso} \sim 10^{50}$–10^{52} erg s^{-1} can just result from the angular structure of the jet. Therefore, following Tan & Yu (2020), the intrinsic LF of SGRBs, which describes the probability distribution of the on-axis luminosity $L_{\rm on}$ of different SGRB jets, is assumed to have a simple power-law form as

$$\Phi(L_{\rm on}) = \Phi_*\left(\frac{L_{\rm on}}{L_{\rm on}^*}\right)^{-\gamma}\exp\left(-\frac{L_{\rm on}^*}{L_{\rm on}}\right), \tag{15}$$

where Φ_* is the normalization coefficient. Then, for an apparent isotropic luminosity $L_{\rm iso}$, its occurring probability should be calculated by integrating over the arbitrary observational directions as

$$p(L_{\rm iso}) = \int\Phi(L_{\rm on}|L_{\rm iso},\,\theta_{\rm obs})\sin\theta_{\rm obs}d\theta_{\rm obs}, \tag{16}$$

where the fact that the jets can be paired is considered. It is assumed that all SGRB jets have the angular profile identical to that of GRB 170817A, but the total energy of the jets and thus the on-axis luminosity can still be different from each other. In the above integration, the value of $\Phi(L_{\rm on}|L_{\rm iso},\,\theta_{\rm obs})$ can be obtained by using Equations (13) or (14) to calculate a value of $L_{\rm on}$ corresponding to the given $L_{\rm iso}$ and $\theta_{\rm obs}$ and, subsequently, substituting the value of $L_{\rm on}$ into the expression of $\Phi(L_{\rm on})$.

3.2. Modeling the Flux and Redshift Distributions of SGRBs

For a comparison with the observational distributions of SGRBs on their fluxes and redshifts, we calculate the model-

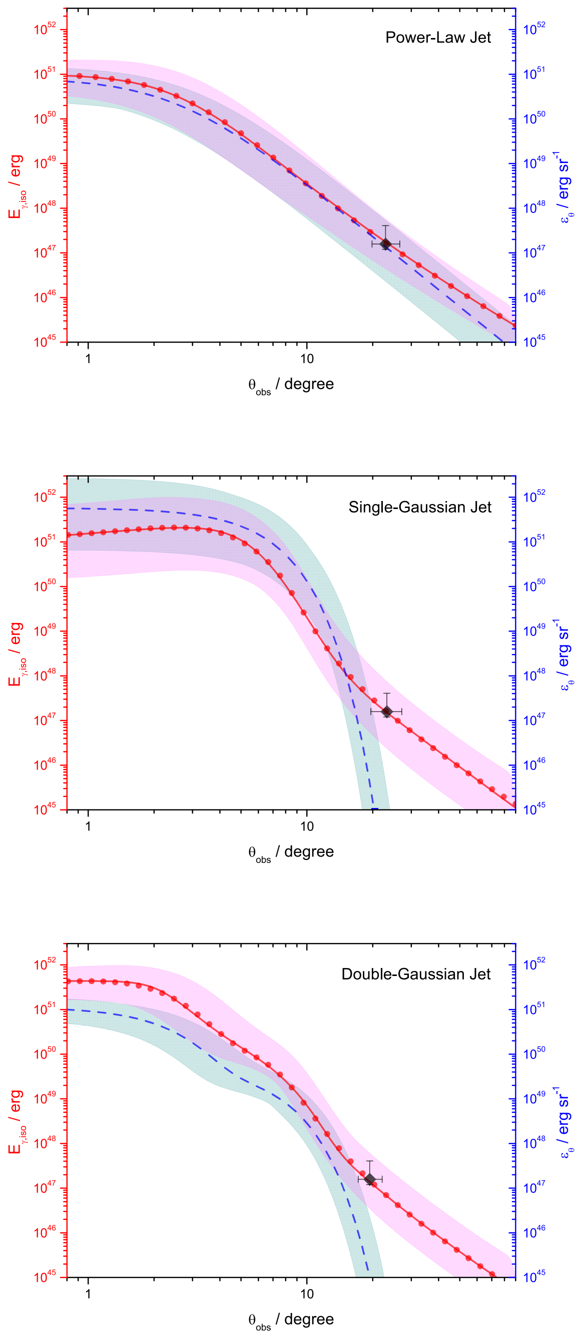

Figure 2. The isotropic emission energy ($E_{\gamma,\mathrm{iso}}$) of SGRBs as a function of viewing angle (solid red line) in comparison with the distribution of the kinetic energy per solid angle (ε_θ; dashed blue line). The solid circles are obtained from Equation (12), while the solid red lines are plotted by timing Equations (13) and (14) to a constant duration of $T = 1$ s, which gives a fit for the solid circles. Here, the central value of the model parameters listed in Table 1 is taken, and the uncertainty arising from the errors of the parameters is represented by the shaded bands. The value of radiation efficiency η_γ is adopted to make the solid line be in agreement with the observational emission energy of GRB 170817A (black diamond).

predicted SGRB numbers in different flux (P) ranges and different redshift (z) ranges by the following integrations (Tan & Yu 2020)

$$N(P_1, P_2) = \frac{\Delta\Omega}{4\pi}\mathcal{T}\int_0^{z_{\max}}\int_{P_1}^{P_2}\eta(P) \times \dot{R}_{\mathrm{SGRB}}(z)p(P)dP\frac{dV(z)/dz}{1+z}dz, \tag{17}$$

and

$$N(z_1, z_2) = \frac{\Delta\Omega}{4\pi}\mathcal{T}\int_{z_1}^{z_2}\int_0^{P_{\max}}\eta(P)\vartheta_z(z, P) \times \dot{R}_{\mathrm{SGRB}}(z)p(P)dP\frac{dV(z)/dz}{1+z}dz, \tag{18}$$

respectively, where $\Delta\Omega$ is the field of view of a telescope, $\mathcal{T}$ is the working time (a duty cycle of $\sim$50% for Fermi should be considered Zhang et al. 2018), $\eta(P)$ and $\vartheta(z, P)$ are the trigger efficiency and the probability of redshift measurement, respectively. In our calculations, the trigger efficiency is considered to increase gradually with the increasing flux, as described by Howell et al. (2014) for the Swift BAT, which reads

$$\eta(P) = \frac{c_1(c_2 + c_3P/P_P^*)}{1 + P/(c_4P_P^*)}, \tag{19}$$

where $c_1 = 0.47$, $c_2 = -0.05$, $c_3 = 1.46$, $c_4 = 1.45$ and $P_P^* = 1.6 \times 10^{-7}$ erg s^{-1} cm^{-2}. However, for the Fermi GBM, such an empirical description is absent, and thus, we have to choose a sufficiently high hard threshold as $P_{\mathrm{th}} = 2.37$ ph s^{-1} cm^{-2} (e.g., Wanderman & Piran 2015). Correspondingly, the low-flux Fermi data is abandoned. Meanwhile, the redshift selection of the Swift BAT can be expressed as (Cao et al. 2011; Tan & Yu 2020)

$$\vartheta(z, P) = \min\left[c_5 + \frac{P}{P_z^*}, 1\right]\exp\left(c_6 - \frac{z}{c_7}\right) \times \left\{1 - c_8\exp\left[-\frac{(z-\mu)^2}{2\sigma^2}\right]\right\} \tag{20}$$

where $c_5 = 0.27$, $c_6 = 0.3$, $c_7 = 8.9$, $c_8 = 0.41$, $P_z^* = 2.0 \times 10^{-6}$ erg s^{-1} cm^{-2}, $\mu = 1.60$, and $\sigma = 0.23$. The occurring probability $p(P)$ of SGRBs can be obtained by substituting the corresponding value of L_{iso} into Equation (16). The relationship between luminosity and flux is given by $L_{\mathrm{iso}} = 4\pi d_{\mathrm{L}}^2 Pk$, where d_{L} is the luminosity distance and k is a correction factor that converts the observational photon flux in the detector band to the energy flux in a fixed rest-frame band of (1, 10^4) keV. More specifically, the calculation of the k − correction involves a tentative value of the peak energy of the Band spectrum (E_{p}) of SGRBs, which can be derived from an

Table 2
Parameters for the Empirical Description of the $E_{\gamma,\rm iso} - \theta_{\rm obs}$ Relation

Model	$L_{\rm on,GRB\ 170817A}$	θ_{b1}	θ_{b2}	θ_{b3}	s	α_1	α_2	α_3	$\mathcal{R}$
Power-law	51	2.5	18	/	0.6	0.	4.3	1.45	/
Single-Gaussian	51.5	6.0	14.3	/	0.4	0.4	9.5	5.9	/
Double-Gaussian	51.62	2.1	22.5	3.65	1.4	0.0	4.9	1.75	0.048

empirical $E_{\rm p} - L_{\rm on}$ correlation as presented in Equation (7) in Tan & Yu (2020). The comoving cosmological volume element in the integration is defined as $dV(z)/dz = 4\pi d_{\rm c}(z)^2 c/H(z)$, where $d_{\rm c}(z) = c\int_0^z H(z')^{-1}dz'$, $H(z) = H_0[(1+z)^3\Omega_{\rm m} + \Omega_\Lambda]^{1/2}$ and the cosmological parameters are taken as $\Omega_{\rm m} = 0.315$, $\Omega_\Lambda = 0.685$, and $H_0 = 67.4\ {\rm km\ s^{-1}\ Mpc^{-1}}$ (Planck Collaboration et al. 2020). Finally, the limit values of the redshift $z_{\rm max}$ and the flux $P_{\rm max}$ are taken according to the boundaries of the observational ranges.

The most crucial input of the above integrations is the cosmic rate of SGRBs, which can usually be connected with the cosmic star formation rates (CSFRs) by a delay time since the SGRBs are produced by mergers of compact binaries, where the delay time is determined by the formation process of the compact binaries and the orbital decay through gravitational radiation. By assuming the delay time τ distributes with a probability function $F(\tau)$, we can express the cosmic SGRB rates by (e.g., Regimbau & Hughes 2009; Zhu et al. 2013; Regimbau et al. 2015):

$$\dot{R}_{\rm SGRB}(z) \propto (1+z)\int_{\tau_{\rm min}}^{t(z)-t(z_{\rm b})} \frac{\dot{\rho}_*[t(z)-\tau]}{1+z[t(z)-\tau]}F(\tau)d\tau \\ \propto (1+z)\int_{z[t(z)-\tau_{\rm min}]}^{z_{\rm b}} \frac{\dot{\rho}_*(z')}{1+z'}F[t(z)-t(z')]\frac{dt}{dz'}dz', \tag{21}$$

where $\dot{\rho}_*(z)$ is the CSFR, $t(z) = \int_z^\infty [(1+z')H(z')]^{-1}dz'$, $dt/dz = -[(1+z)H(z)]^{-1}$, and $z_{\rm b}$ represents the redshift at which the binaries started to be formed. Finally, please see Cao et al. (2011) and Tan & Yu (2020) for the details of the expressions of k, $\dot{\rho}_*(z)$, and $F(\tau)$.

Assigning values for parameters γ, $L_{\rm on}^*$, and τ, we generate a number of 10^5 simulated SGRB samples according to the occurring probability given by Equations (16) and (21). Then, we can obtain the number distributions of these mocked samples on their redshifts or fluxes and, furthermore, compare these distributions with the observational ones. Finally, the value of $\dot{R}_{\rm SGRB}(0)$ is determined by normalizing the mocked distributions by the total number of Swift SGRBs. Here, for the Swift SGRBs, we extract their 1 s peak photon fluxes in the 15–150 keV energy range from https://swift.gsfc.nasa.gov/results/batgrbcat/index.html, up until 2023. Meanwhile, for the Fermi SGRBs, their 64 ms peak photon fluxes in the energy band of 50–300 keV have been provided at https://heasarc.gsfc.nasa.gov/W3Browse/fermi/fermigbrst.html, where the data is updated until 2018. In principle, these peak fluxes can be somewhat different from the average ones we used in the model, which is nevertheless not very significant for a short period of $T \sim 1$ s for the average ones. Furthermore, considering that the difference between the peak and average fluxes can actually be coupled with and then included into the assumed constant value of T, we ignored this difference in our calculations for simplicity. The best fit of the observational distributions, which is presented in Figures 3, 4, and 5 for the three jet structures, is obtained by minimizing the sum of χ^2 of the redshift and flux distributions. Here, we calculate $\chi^2 = \sum_{i=1}^n \frac{(O_i - M_i)^2}{M_i}$ with O_i and M_i being the observational and simulated SGRB numbers, respectively, in the corresponding redshift or flux bins. The priors and posteriors of our simulations are listed in Table 3. Finally, as indicated by the KS tests of the best fits, the single-Gaussian model could be relatively disfavored by the peak flux distribution for the Fermi data, even though the large-angle emission effect is taken into account. In comparison, the goodness of the power-law and double-Gaussian models is comparable to each other (the latter is relatively better). With the obtained values of the intrinsic LF parameters, the typical delay time, and the total rates of SGRBs, we plot the luminosity dependence of the event rates of the SGRBs (e.g., the apparent LF) in Figure 6, compared to the event rate of $190^{+440}_{-160}\ {\rm yr^{-1}\ Gpc^{-3}}$ inferred by GRB 170817A (Zhang et al. 2018). As shown, the power-law structure can determine an event rate for $L_{\rm iso} \gtrsim 10^{47}\ {\rm erg\ s^{-1}}$ well consistent with the central value of the GRB 170817A rate, whereas the double-Gaussian model can only reach the marginal value of the error range.

4. Summary

The uncovering of the jet structure is one of the most crucial aims of the GRB research, which can help to understand the nature of their progenitors and central engines. It has long been expected to constrain the jet structure by using the observed afterglow emission. However, usually, only an effective half-opening angle of the jet can be derived from the data if a so-called jet-break characteristic can be identified from the afterglow light curves. The discovery of GRB 170817A had changed this awkward situation, because it was significantly

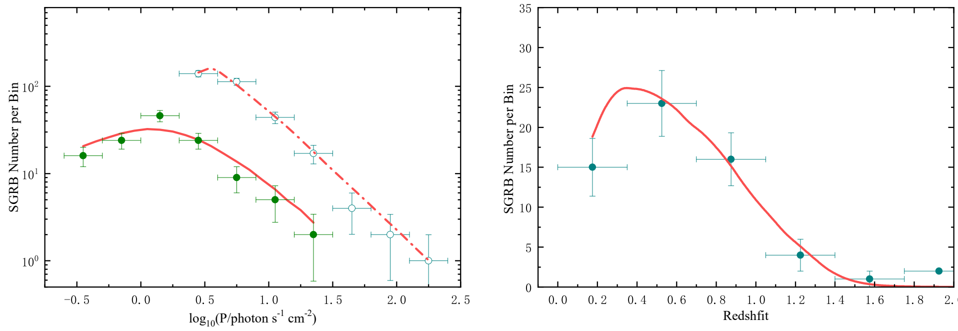

Figure 3. Comparison between the model-predicted and observational flux and redshift distributions of SGRBs for a power-law jet structure. The solid and open data circles are the results of the Swift and Fermi observations, respectively.

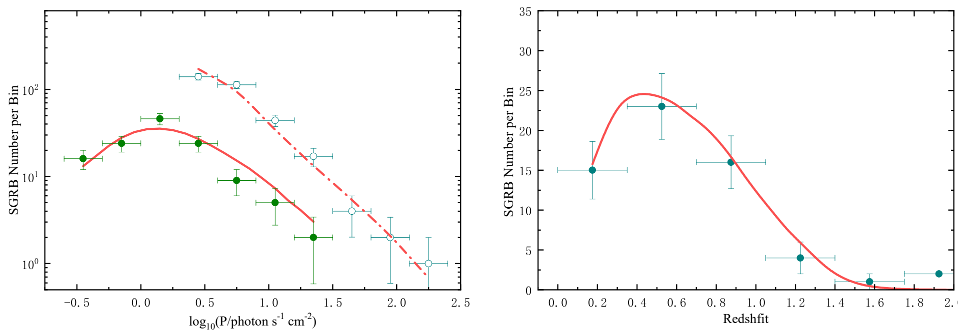

Figure 4. Same as Figure 3 but for a single-Gaussian jet structure.

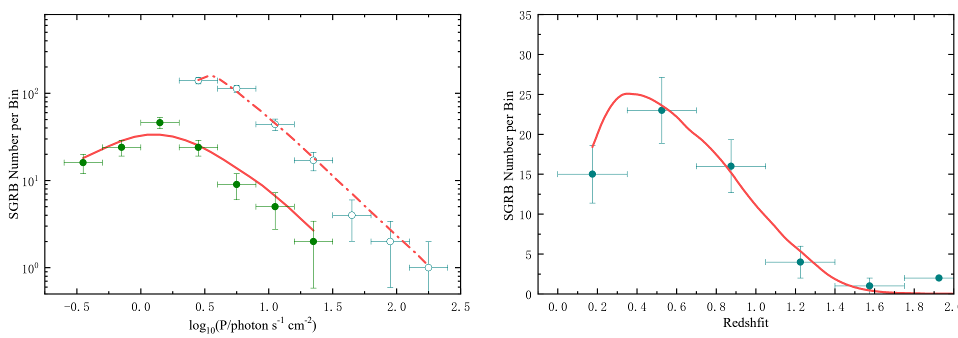

Figure 5. Same as Figure 3 but for a double-Gaussian jet structure.

Table 3
Constraints on the Luminosity Function and Event Rates of SGRBs

Parameter	Prior	Posterior		
		Power-Law	Single-Gaussian	Double-Gaussian
γ	(1, 3)	$2.37^{+0.73}_{-0.64}$	$2.41^{+1.27}_{-0.65}$	$2.25^{+1.66}_{-0.42}$
$L^*_{\rm on}/10^{52}$ erg s^{-1}	(0.1, 10)	$2.08^{+2.14}_{-1.22}$	$2.62^{+2.23}_{-1.36}$	$0.56^{+0.68}_{-0.33}$
$\tau_{\rm min}$/Gyr	(1, 5)	$3.02^{+0.44}_{-0.55}$	$3.01^{+0.44}_{-0.55}$	$2.94^{+0.44}_{-0.55}$
$\dot{R}_{\rm SGRB}(0)/{\rm Gpc}^{-3}$ yr^{-1}	…	$325.96^{+39.46}_{-20.59}$	$112.07^{+12.98}_{-8.26}$	$454.01^{+50.18}_{-33.46}$
$P^{\rm Fermi}_{{\rm KS},F}$	…	0.23	2.76×10^{-4}	0.20
$P^{\rm Swift}_{{\rm KS},F}$	…	0.13	0.14	0.30
$P_{{\rm KS},z}$	…	0.78	0.62	0.83

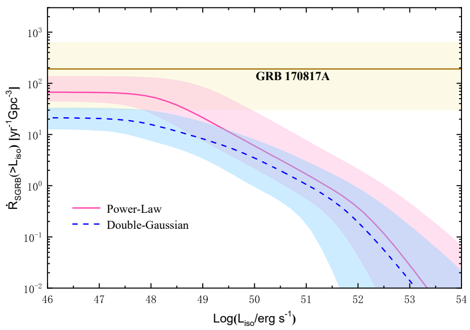

Figure 6. The apparent LF given by the power-law and the double-Gaussian jet models, in comparison with the event rate 190^{+440}_{-160} yr^{-1} Gpc^{-3} inferred from the GRB 170817A observations represented by the shaded band (Zhang et al. 2018).

observed off-axis. Then, an immediate question is whether the jet structures inferred from the afterglows of GRB 170817A can be compatible with the statistical properties of the SGRB population, if it is assumed that all SGRBs, including GRB 170817A, have a common origin and explosive mechanism. Therefore, in this paper, we investigate three typical empirical jet structures, including the power-law, single-Gaussian, and double-Gaussian cases, the parameters of which are first constrained according to the afterglow data of GRB 170817A. It is further demonstrated that these three types of jet structure can all account for the prompt luminosity of GRB 170817A, with the consideration of the large-angle emission effect of relativistic jets. However, the single-Gaussian structure could somewhat fail to reproduce the flux distribution for the Fermi data. By comparison, the power-law structure is more favored by the statistical results and, furthermore, predicts an event rate closer to the value inferred from GRB 170817A. Nevertheless, it should be kept in mind that the large number of model parameters could still make these conclusions subject to the large uncertainty of the parameters.

Acknowledgments

This work is supported by the National Key R&D Program of China (2021YFA0718500), the China Manned Spaced Project (CMS-CSST-2021-A12), the National Natural Science Foundation of China (grant Nos. 12393811, U1838203, and 11803007), and Hubei Provincial Outstanding Young and Middle-aged Science and Technology Innovation Team Project of China (T2021026).

References

Abbott, B. P., Abbott, R., Abbott, T. D., et al. 2017a, ApJL, 848, L13
Abbott, B. P., Abbott, R., Abbott, T. D., et al. 2017b, PhRvL, 119, 161101
Beniamini, P., Granot, J., & Gill, R. 2020, MNRAS, 493, 3521
Beniamini, P., & Nakar, E. 2019, MNRAS, 482, 5430
Bromberg, O., Granot, J., Lyubarsky, Y., & Piran, T. 2014, MNRAS, 443, 1532
Bromberg, O., Nakar, E., Piran, T., & Sari, R. 2011, ApJ, 740, 100
Cao, X.-F., Yu, Y.-W., Cheng, K. S., & Zheng, X.-P. 2011, MNRAS, 416, 2174
Dai, Z. G., & Gou, L. J. 2001, ApJ, 552, 72
D'Avanzo, P., Campana, S., Salafia, O. S., et al. 2018, A&A, 613, L1
Fong, W., Blanchard, P. K., Alexander, K. D., et al. 2019, ApJL, 883, L1
Foreman-Mackey, D., Hogg, D. W., Lang, D., & Goodman, J. 2013, PASP, 125, 306
Garcia-Cifuentes, K., Becerra, R. L., De Colle, F., & Vargas, F. 2024, MNRAS, 527, 6752
Ghirlanda, G., Salafia, O. S., Pescalli, A., et al. 2016, A&A, 594, A84
Gill, R., & Granot, J. 2018, MNRAS, 478, 4128
Gottlieb, O., & Nakar, E. 2022, MNRAS, 517, 1640
Granot, J., Gill, R., Guetta, D., & De Colle, F. 2018, MNRAS, 481, 1597
Granot, J., & Kumar, P. 2003, ApJ, 591, 1086
Granot, J., & Piran, T. 2012, MNRAS, 421, 570
Granot, J., & Sari, R. 2002, ApJ, 568, 820
Hamidani, H., & Ioka, K. 2021, MNRAS, 500, 627
Hayes, F., Heng, I. S., Lamb, G., et al. 2023, ApJ, 954, 92
He, X.-B., Tam, P.-H. T., & Shen, R.-F. 2018, RAA, 18, 043
Howell, E. J., Coward, D. M., Stratta, G., Gendre, B., & Zhou, H. 2014, MNRAS, 444, 15
Huang, B.-Q., Lin, D.-B., Liu, T., et al. 2019, MNRAS, 487, 3214
Huang, Y. F., Dai, Z. G., & Lu, T. 1999, MNRAS, 309, 513
Huang, Y. F., Gou, L. J., Dai, Z. G., & Lu, T. 2000, ApJ, 543, 90
Kathirgamaraju, A., Tchekhovskoy, A., Giannios, D., & Barniol Duran, R. 2019, MNRAS, 484, L98
Kumar, P., & Granot, J. 2003, ApJ, 591, 1075
Lamb, G. P., & Kobayashi, S. 2017, MNRAS, 472, 4953
Lamb, G. P., Lyman, J. D., Levan, A. J., et al. 2019, ApJL, 870, L15
Lazzati, D., & Begelman, M. C. 2005, ApJ, 629, 903
Lazzati, D., López-Cámara, D., Cantiello, M., et al. 2017, ApJL, 848, L6
Lazzati, D., Perna, R., Morsony, B. J., et al. 2018, PhRvL, 120, 241103
Li, Y.-S., Chen, A., & Yu, Y.-W. 2019, RAA, 19, 115
Luo, J.-W., Li, Y., Ai, S., Gao, H., & Zhang, B. 2022, MNRAS, 516, 1654
Makhathini, S., Mooley, K. P., Brightman, M., et al. 2021, ApJ, 922, 154
Margutti, R., Alexander, K. D., Xie, X., et al. 2018, ApJL, 856, L18
Margutti, R., Berger, E., Fong, W., et al. 2017, ApJL, 848, L20
Matzner, C. D. 2003, MNRAS, 345, 575
Medvedev, M. V. 2006, ApJL, 651, L9
Meliani, Z., & Keppens, R. 2010, in ASP Conf. Ser. 429, Numerical Modeling of Space Plasma Flows, Astronum-2009, ed. N. V. Pogorelov, E. Audit, & G. P. Zank (San Francisco, CA: ASP), 121
Mooley, K. P., Frail, D. A., Dobie, D., et al. 2018, ApJL, 868, L11
Morsony, B. J., De Los Santos, R., Hernandez, R., et al. 2024, MNRAS, 533, 510
Nagakura, H., Hotokezaka, K., Sekiguchi, Y., Shibata, M., & Ioka, K. 2014, ApJL, 784, L28
Nakar, E., & Piran, T. 2021, ApJ, 909, 114
Nathanail, A., Gill, R., Porth, O., Fromm, C. M., & Rezzolla, L. 2021, MNRAS, 502, 1843
Nativi, L., Lamb, G. P., Rosswog, S., Lundman, C., & Kowal, G. 2022, MNRAS, 509, 903
Nynka, M., Ruan, J. J., Haggard, D., & Evans, P. A. 2018, ApJL, 862, L19
Pavan, A., Ciolfi, R., Kalinani, J. V., & Mignone, A. 2023, MNRAS, 524, 260
Planck Collaboration, Aghanim, N., Akrami, Y., et al. 2020, A&A, 641, A6
Regimbau, T., & Hughes, S. A. 2009, PhRvD, 79, 062002
Regimbau, T., Siellez, K., Meacher, D., Gendre, B., & Boër, M. 2015, ApJ, 799, 69
Resmi, L., Schulze, S., Ishwara-Chandra, C. H., et al. 2018, ApJ, 867, 57
Rossi, E., Lazzati, D., & Rees, M. J. 2002, MNRAS, 332, 945
Rossi, E. M., Lazzati, D., Salmonson, J. D., & Ghisellini, G. 2004, MNRAS, 354, 86
Rybicki, G. B., & Lightman, A. P. 1979, Radiative Processes in Astrophysics (New York: Wiley)
Salafia, O. S., Barbieri, C., Ascenzi, S., & Toffano, M. 2020, A&A, 636, A105
Salafia, O. S., & Ghirlanda, G. 2022, Galax, 10, 93

Salafia, O. S., Ghisellini, G., Pescalli, A., Ghirlanda, G., & Nappo, F. 2015, MNRAS, 450, 3549
Sari, R., Piran, T., & Narayan, R. 1998, ApJL, 497, L17
Suwa, Y., & Ioka, K. 2011, ApJ, 726, 107
Takahashi, K., & Ioka, K. 2020, MNRAS, 497, 1217
Takahashi, K., & Ioka, K. 2021, MNRAS, 501, 5746
Tan, W.-W., & Yu, Y.-W. 2020, ApJ, 902, 83
Troja, E., Piro, L., van Eerten, H., et al. 2017, Natur, 551, 71
Troja, E., Piro, L., Ryan, G., et al. 2018, MNRAS, 478, L18
Urrutia, G., De Colle, F., & López-Cámara, D. 2023a, MNRAS, 518, 5145
Urrutia, G., De Colle, F., Moreno, C., & Zanolin, M. 2023b, MNRAS, 518, 5242
van Eerten, H., Zhang, W., & MacFadyen, A. 2010, ApJ, 722, 235
Wanderman, D., & Piran, T. 2015, MNRAS, 448, 3026
Wei, F., Zhang, Z.-D., Yu, Y.-W., & Liu, L.-D. 2022, SSPMA, 52, 129511
Xiao, D., Liu, L.-D., Dai, Z.-G., & Wu, X.-F. 2017, ApJL, 850, L41
Xie, X., Zrake, J., & MacFadyen, A. 2018, ApJ, 863, 58
Yu, Y.-W. 2020, ApJ, 897, 19
Yu, Y.-W., Gao, H., Wang, F.-Y., & Zhang, B.-B. 2022, in Handbook of X-ray and Gamma-ray Astrophysics, ed. C. Bambi & A. Sangangelo (Singapore: Springer)
Yu, Y. W., Liu, X. W., & Dai, Z. G. 2007, ApJ, 671, 637
Zhang, B. B., Zhang, B., Sun, H., et al. 2018, NatCo, 9, 447
Zhang, B., & Mészáros, P. 2002, ApJ, 571, 876
Zhang, W., & MacFadyen, A. 2009, ApJ, 698, 1261
Zhang, W., Woosley, S. E., & MacFadyen, A. I. 2003, ApJ, 586, 356
Zhu, X.-J., Howell, E. J., Blair, D. G., & Zhu, Z.-H. 2013, MNRAS, 431, 882
Ziaeepour, H. 2019, MNRAS, 490, 2822